City Research Online

City St George's, University of London

Citation: Jin, Q., He, D., Cao, X., Fu, F., Chen, Y., Zhang, M. & Ren, Y. (2024). Shear strength prediction of high strength steel reinforced reactive powder concrete beams. Advances in Concrete Construction, 17(2), pp. 75-92. doi: 10.12989/acc.2024.17.2.072

This is the accepted version of the paper.

This version of the publication may differ from the final published version. To cite this item please consult the publisher's version.

Permanent repository link: https://openaccess.city.ac.uk/id/eprint/33468/

Link to published version: https://doi.org/10.12989/acc.2024.17.2.072

Copyright and Reuse: Copyright and Moral Rights remain with the author(s) and/or copyright holders. Copies of full items can be used for personal research or study, educational, or not-for-profit purposes without prior permission or charge, unless otherwise indicated, provided that the authors, title and full bibliographic details are credited, a hyperlink and/or URL is given for the original metadata page and the content is not changed in any way. For full details of reuse please refer to City Research Online policy.

City Research Online: http://openaccess.city.ac.uk/ publications@citystgeorges.ac.uk

Shear strength prediction of High Strength steel reinforced Reactive Powder Concrete Beams

Qi-Zhi Jin[1], Da-Bo He[2], Xia Cao[*1], Feng Fu[*3], Yi-Cong Chen[4], Meng Zhang[5], Yi-Cheng Ren[6]

[1]*Guangxi Key Laboratory of Green Building Materials and Construction Industrialization, Guilin University of Technology, Guilin 541004, China.*
[2]*School of Civil Engineering, Nanning College of Technology, Guilin, China, 541006, China.*
[3]*Department of Engineering, School of Science & Technology, City, University of London, EC1V 0HB, U.K.*
[4]*College of Civil Engineering, Fuzhou University, Fuzhou, 350116, China.*
[5]*Infrastructure construction department, Guilin University of Technology, Guilin, 541004, China.*
[6]*Jiangsu University Jingjiang College, Jiangsu, 212028, China*

(Received , Revised , Accepted)

Abstract. High Strength steel reinforced Reactive Powder Concrete (RPC) Beam is a new type of beams which has evident advantages than the conventional concrete beams. However, there is limited research on the shear bearing capacity of high-strength steel reinforced RPC structures, and there is a lack of theoretical support for structural design. In order to promote the application of high-strength steel reinforced RPC structures in engineering, it is necessary to select a shear model and derive applicable calculation methods. By considering the shear span ratio, steel fiber volume ratio, longitudinal reinforcement ratio, stirrup ratio, section shape, horizontal web reinforcement ratio, stirrup configuration angle and other variables in the shear test of 32 high-strength steel reinforced RPC beams, the applicability of three theoretical methods to the shear bearing capacity of high-strength steel reinforced RPC beams was explored. The plasticity theory adopts the RPC200 biaxial failure criterion, establishes an equilibrium equation based on the principle of virtual work, and derives the calculation formula for the shear bearing capacity of high-strength steel reinforced RPC beams; Based on the Strut and Tie Theory, considering the softening phenomenon of RPC, a failure criterion is established, and the balance equation and deformation coordination condition of the combined force are combined to derive the calculation formula for the shear bearing capacity of high-strength reinforced RPC beams; Based on the Rankine theory and Rankine failure criterion, taking into account the influence of size effects, a calculation formula for the shear bearing capacity of high-strength reinforced RPC beams is derived. Experimental data is used for verification, and the results are in good agreement with a small coefficient of variation.

Keywords: reactive powder concrete, high strength reinforcement, plastic theory, strut and tie, rankine theory, span to depth ratio, reinforcement ratio, stirrup ratio, section shape

1. Introduction

Reactive Powder Concrete (RPC) which is also called ultra-high-performance concrete (UHPC) is a special concrete with microstructure optimized by precise gradation of all particles in the mix to yield maximum density (Hoang et al, 2017, Ghosh et al.2017). It is composed of very fine powders (cement, sand, quartz powder and silica fume), steel fibers (optional) and superplasticizer. Due to its high strength, good workability and high durability, it has been successfully used for buildings and bridges in the past decades. It is particularly used for structure to store containment of nuclear wastes in Europe due to its excellent impermeability (Lai, et al. 2010, Deng et al. 2014, Nematzadeh et al, 2017, Poorhosein et al,2018). High strength reinforcement has high strength and good plastic deformation properties. The combination of RPC and high strength reinforcement can fully exploit their respective advantages. Currently, some research has been done on investigating the structural behavior of this type of structures, but there are no pertinent design guidelines available for the practicing engineers.

The shear behaviour of high-performance concrete is still not sufficient. Marcinczak et al. (2019) investigated on the shear strengthening of reinforced concrete beams with PBO-FRCM composites with anchorage. Tung et al. (2018) investigated the shear resistance of steel fiber-reinforced concrete beams without conventional shear reinforcement on the basis of the critical shear band concept. Ridha et al (2018) developed equations which gave satisfied predictions for the shear strength of the tested RPC beams. Tamás et al (2018) made investigation on the effect of the traditional transverse shear reinforcement and the effect of the fiber reinforcement on the shear behavior as well as 6 High-Performance Fiber-Reinforced Concrete (HPFRC) I-beams. Talayeh et al (2014) putted forward an elastic-plastic fictitious RU-RC composite hinge model for the damage caused by flexural and flexure-shear cracks in the RC element of the composite members, which can accurately predict the member response, resistance and failure mode.

[*1]Corresponding author, Professor
E-mail: email address: 2002015@glut.edu.cn
[*3]Corresponding author, Senior Lecturer
E-mail: email address: cenffu@yahoo.co.uk

Lim et al (2016) investigated on considering the failure mechanisms and the shear capacity of UHPC. Jenny et al (2016) analyzed the shear capacity of ten UHPC-beams with combined reinforcement, and the existing shear bearing models are analyzed and considered in this paper. Baby et al (2014) developed design provisions and model. Baby et al (2014) putted forward improved models for serviceability-limit states prediction and realistic accounting of critical shear-crack. Pansuk et al (2017) investigate on the shear capacity of UHPFRC rectangular cross-sectional beams with fiber dosage of 1.5 % considering a spacing of shear reinforcement.

Xia (2007) proposed a calculation equation for the shear capacity of RPC beams under different Shear span-to-effective depth ratios, stirrups, longitudinal ratios, RPC strength and prestress force based on the softened truss model, it is analysed and verified using finite element models. Kang (2012) used the soft truss model to analyse the beam under different Shear span-to-effective depth ratios, stirrups, longitudinal ratios, concrete strength and flange width using ANSYS software, and finally revised the existing shear capacity equation from design specification and proposed the new one. Deng et al. (2014) proposed an improved compression stress theory based on the experimental study of T-section high-strength stirrup RPC beams. The effects of varying rebar buried length, thickness of protective layer and diameter of rebars on the bonding properties were studied. The theory considers the shearing enhancement due to the of steel fibress at cracks. Chen (2007) also studied the prestressed RPC beams under different Shear span-to-effective depth ratios, stirrups and prestress force based on plasticity theory, and proposed the shear capacity of prestressed RPC beams. In 2009, Wu el al (2009) developed the upper bound and lower bound equation in plastic theory for RPC beam based on shear failure test analysis, considering the role of steel fibres. Yan (2011) conducted a statistical analysis based on the shear test of the RPC beam, they proposed an empirical equation for the shear strength, and verified the reliability of the equation based on the ANSYS software. Jin et al (2019). conducted a series of shear test studies on four large girders (one SFR-RPC girder and three post-tensioned SFR-RPC girders) to quantify the effect of prestressing level on the shear load capacity of SFR-RPC girders. And equation for calculating the shear load capacity is also proposed. Baby et al. (2013) adopted the Modified Compression Field Theory (MCFT) to grasp the flexure-shear behavior of prestressed or reinforced beams made of Ultra High Performance Fiber-Reinforced Concrete (UHPFRC), and the predictions of the model agree rather well with the experimental results .Sifatullah et al (2018) conducted the numerical model to analyze the shear behavior of ultra-high-performance concrete (UHPC) beams reinforced longitudinally with high-strength rebars and ordinary-strength steel (stirrups), and the results showed that it match well with the experimental data and can predict the response of the beam with variation in various parameters with a good accuracy. Voo et al (2006, 2010) conducted the plastic shear variable engagement predictive model to analyze the shear strength of steel fiber reinforced UHPC beams. The study shows this model is appropriate for the determination of the shear strength of steel fiber reinforced UHPC beams with steel fibers. Qi et al (2017) conducted the mesoscale fiber-matrix discrete model (MFDM) to estimate the shear contribution of steel fibers and calculating shear strength of ultrahigh-performance fiber-reinforced concrete (UHPFRC) beams. In the proposed model, an effective fiber distributed region (EDR) along the critical diagonal shear crack, where fibers are efficient at providing shear resistance, is defined. The total quantity of fibers within EDR is calculated by the EDR volume proportion of the beam based on a uniform distribution of steel fibers. Two concepts to determine the width of EDR are proposed: (1) probability theory and (2) the basis of the pullout load slip relationship. Pourbaba et al (2018) proved that theoretical shear strengths, determined by RILEM equations for UHPC beams, is very conservative, and more accurate assessment of shear strength of UHPC is needed.

From above literature reviews, it can be seen that, due to its complicated mechanism and various influencing factors, though some researchers such as Ridha et al. (2018) developed the equation for shear prediction for RPC beams, no available calculation methods for the shear capacity of HSR reinforced RPC beams have ever been developed up to date. Therefore, in this paper, detailed investigation on the shear capacity of this new type of beam is made. Based on the findings from full scale tests as well as theoretical derivation were conducted. Three existing theories (Plastic theory, Strut and Ties theory, Rankine theory) were used for the derivation of new equations. The calculation methods for the shear capacity of this new type of beams were first time developed. The proposed calculation methods were validated against the test results, the accuracies of the proposed methods were assessed. It shows that all of them can be confidently used for shear capacity calculations.

2. Full scale shear Test

As it is shown in Fig. 1, Twenty-three full scale shear tests were performed for HSR reinforced RPC beams (Cao et al, 2019). The effect of the shear span to effective depth ratio, the ratio of longitudinal reinforcement, stirrup ratio, web reinforcement ratio, dosage of the steel fiber, section shape and shear stirrup configuration angle on the shear capacity of HSR reinforced RPC concrete were studied in detail.

Fig. 2 shows the test set up and the location of the instrumentation. The total span of the beam is 2200 mm, with the clear span varied for each test. This span length is chosen to make sure shear failure will be observed during the test. The load is applied through a loading frame, the location of instrumentations such as the dial gauges are shown in Fig. 1.

2.1 Test specimens and Material properties

High strength steel bars with grade HRB500 and HRB400 as well as addition of different dosage of steel fiber were used in the beams. Grade PO 42.5 Portland

cement and Quartz sand with three different gradation is used as the coarse, medium and fine aggregate with the addition of silicon powder. In addition, water reducer with about 20% of polycarboxylate superplasticizer is added into the mix, which accounts 0.1% of cement mix. The detailed mix design and mechanical properties of each composition are shown in Table 1-4, Key parameters of test beam are shown in Table 5 for and detailed reinforcement drawing of section are shown in Fig. 3.

In order to study the influence of shear span ratio, longitudinal reinforcement ratio and stirrup ratio on the shear performance of reactive powder concrete, 23 test beams were designed and manufactured for shear performance test specific parameters of the test beams are shown in Table 5 and Fig. 3. *a* is the shear span length and 1800-2*a* is the pure bending section length.

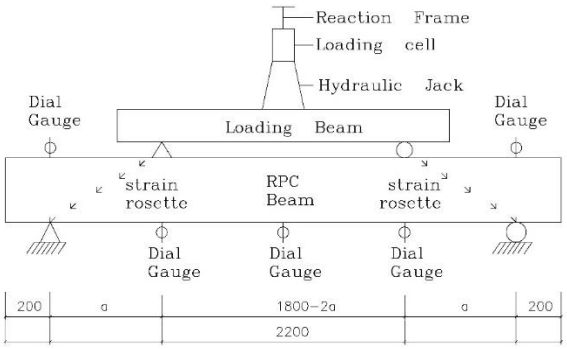

Fig. 1 Test setup and instrumentation

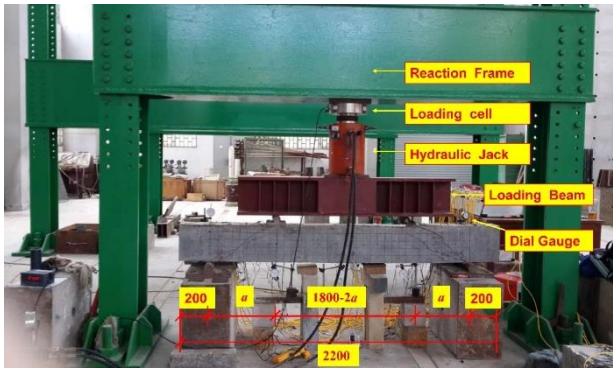

Fig. 2 Schematic drawing of test set up

Table 1 Shear strength models of RPC/UHPC beams for different proposed equations

Source	Shear strength models	Parameters
Chen (2007)	$V=\left(\frac{1.5}{l}+0.5\right)a_1\sqrt{f_c}bh_0+r_{sv}f_{sv}bh_0+\frac{0.09}{l}N_{p0}$ $a_1=1+(b_f/b-1)(27r_{sv}-0.21)$	λ is the shear span to depth ratio (λ=1.5 for λ<1.5, λ=3.0 for λ>1.5); f_c is the cubic compressive strength ; α_1 is flange width enhancement coefficient, and reinforced concrete is taken as 1.0; ρ_{sv} is the stirrup ratio f_{sv} is the yield strength of stirrup; b_f/b is ratio of flange width to web width.
Kang (2012)	$V=\frac{2.53}{l+0.89}(1.31+5.38r_s)(1+\frac{A_p}{bh_0})f_tbh_0$ $+(1.26+0.15l)r_{sv}f_{sv}bh_0$	ρ_s is the longitudinal reinforcement ratio; A_p is effective area of upper flange; f_t is the cubic tensile strength; same parameters as above.
Voo et al (2006)	$V_u=\frac{1}{2}f_cbh\left(\sqrt{1+\left(\frac{x}{h}\right)^2}-\frac{x}{h}\right)$	where f_c is the effective concrete strength, b and h are the width and depth of the section, respectively, and x is the horizontal projection of the yield line.
Jin (2019)	$V_u=\left(\frac{0.07}{\lambda-0.852}+\frac{49.086\rho_s}{f_{cc}}\right)f_{cc}b_wd(1+\beta_f\rho_f)$ $(0.755+0.054A_d)+\frac{A_{sv}f_{yv}z}{s}$	λ is the shear span to depth ratio; f_{cc} is cylinder compressive strength; β_f is the influence coefficient of steel fiber on shear strength; ρ_f is the volume ratio of steel fiber; A_d is the shape adjustment factor ($A_d=\lambda$ for $1.0<\lambda<2.5$, $A_d=2.5$ for $\lambda\geq2.5$).

Table 2 Mix ratio of reactive Powder concrete

Mix ratio 1	Cement	Quartz sand	Quartz powder	silica fume	silicon powder	components	Water reducer	water	Steel fibres
	1.0	0.9	0.2	0.35	0.35	0.1	0.015	0.25	2%
Mix ratio 2	Cement	Quartz sand(Coarse)	Quartz sand(Medium)	Quartz sand(fine)	silicon powder	Water reducer	water	Steel fibres	
	1.0	0.2	0.8	0.2	0.30	0.02	0.23	2%	

Note：Steel fibres use volume ratio, the remaining component use mass ratio; Components include expansion agent, polyester fiber and latex protein.

Table 3 Mechanical properties of RPC concrete

Mix ratio	Cubic compressive strength f_{cu}/Mpa	Cylindrical compressive strength f_c/Mpa	Tensile splitting strength f_{ts}/Mpa	Young's modulus/Mpa
Mix ratio 1	127.10	117.20	6.89	4.2×10^4
Mix ratio 2	147.8	126.2	7.25	4.5×10^4

Table 4 The mechanical properties of steel bar

Type of Rebar	Diameter /mm	Yield strength /MPa	Ultimate strength /MPa	Young's modulus /MPa
HRB500	25	555.9	735.7	2×10^5
HRB400	6	466.3	657.3	2×10^5

Table 5 Key parameters of tested beams and Failure pattern

Beam	λ	Longitudinal rebar	ρ_s/%	Stirrup	ρ_{sv}/%	ρ_{sh}/%	ρ_f/%	θ_{sv}/°
LL1	2.25	4D25	6.58	—	0	0	2	—
LL2	2.25	4D25	6.58	C6@225	0.17	0	2	90
LL3	2.25	4D25	6.58	C6@150	0.25	0	2	90
LL4	2.25	4D25	6.58	C6@65	0.58	0	2	90
LP1	2.25	3D25	4.48	—	0	0	2	—
LP2	2.25	5D25	8.18	—	0	0	2	—
LH1	1.5	4D25	6.58	—	0	0	2	—
LH2	3	4D25	6.58	—	0	0	2	—
LZ1	1	5D25	8.18	—	0	0	2	—
LZ2	2.25	5D25	8.18	—	0	0	2	—
LZ3	3.5	5D25	8.18	—	0	0	2	—
LZ4	1.5	5D25	8.18	C6@150	0.25	0	2	90
LZ5	2.25	5D25	8.18	C6@150	0.25	0	2	90
LZ6	3	5D25	8.18	C6@150	0.25	0	2	90
LC1	2.25	5D25	8.18	C6@75	0.50	0	2	90
LC2	3	5D25	8.18	C6@300	0.13	0	2	90
LC3	3	5D25	8.18	C6@100	0.38	0	2	90
LY1	3.5	5D25	8.18	—	0	0	2	—
LY2	2.25	5D25	8.18	—	0	0	2	—
LY3	2.25	5D25	8.18	C6@150	0.25	0	2	90
LT1	1.5	4D25	6.58	C6@150	0.25	0	2	90
LT2	1.5	6D25	9.87	C6@150	0.25	0	2	90
LT3	2.25	6D25	9.87	C6@150	0.25	0	2	90

NB: LY1、 LY2 and LY3 are T-shaped, the other test beams are rectangular shape, λ is shear span ratio, ρ_s is longitudinal reinforcement ratio, ρ_{sv} is stirrup ratio, ρ_{sh} is the ratio of the web reinforcement , ρ_f is the dosage of steel fibres , θ_{sv} is the angle of the stirrup. Test beams are poured and tested in three batches, separated by horizontal lines, which are the same as below; In addition to the mixture ratio of LT1、LT2、LT3, the other mixture ratio of 2.

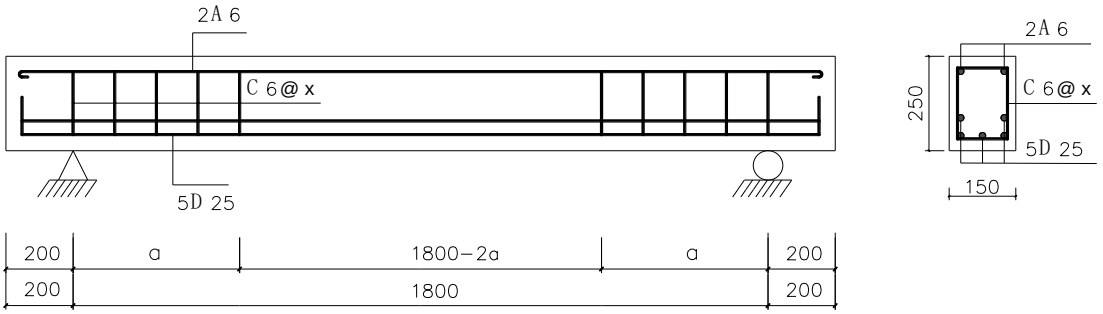

(a)Reinforcement drawing of test beam without and with web reinforcement

(Note: C6@150 denotes a double limb stirrup with a diameter of 6mm spacing of 150mm.; The stirrup spacing x is taken 65、75、150、220 and 300 mm)

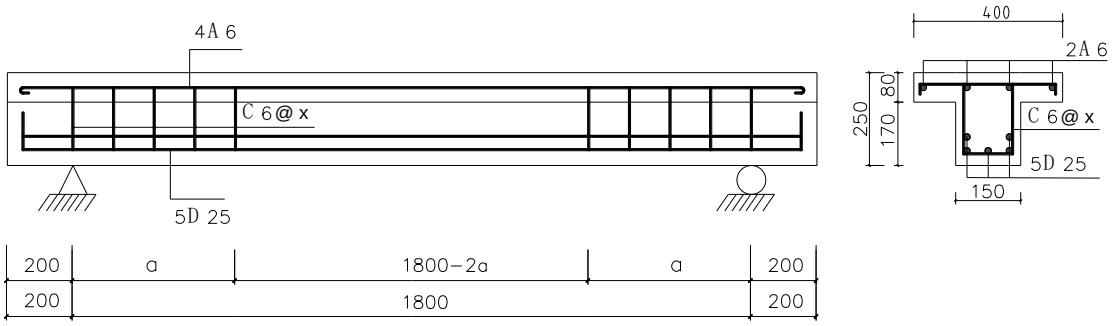

(b)Reinforcement drawing of T test beam without and with web reinforcement

(The stirrup spacing x is taken 150 mm)

Fig. 3 Details of test beam

(a)Reinforcing cage

(b)timber forms

(c)Pressurization around timber forms

(d)Vibrating table vibration

Fig. 4 Manufacturing process of test beam

2.2 Manufacture of test teams

The manufacturing process of high-strength reinforced RPC beam is as follows：

(1) Steel bars. First, polish the steel bar and stick the strain gauge according to the plan, then wrap the strain gauge with gauze containing epoxy resin, take waterproof protection measures, and finally tie the reinforcing cage are shown in Fig. 4(a).

(2) Timber forms. According to the test design and the actual reinforcing cage size, make the specimens timber forms. The upper part of the specimen timber forms are reinforced with wooden strips to prevent the timber forms from expanding are shown in Fig. 4(b).

(3) Pouring. Weigh the materials according to the mixture ratio, pour quartz sand, steel fiber, cement, silica fume and other materials into a forced mixer for dry mixing, mix well for 4~5 minutes, add water reducer and water, continue mixing for 4 minutes, and then pour test beams and test blocks. When pouring, the test beam is vibrated with a vibrator, and the periphery of the template is beaten and pressurized to enrich the RPC pouring; The test block shall be vibrated by vibrating table for 4~5 minutes. Finally, the beams and test blocks are plastered and compacted are shown in Fig. 4(c).

(4) Maintenance. Maintenance is divided into normal temperature maintenance and high temperature maintenance. The test beams and test blocks shall be poured after standing for 24 hours, and the normal temperature curing temperature is about 25℃. Then put it into a curing pool for high temperature curing for 3 days at 65℃. Finally, curing at normal temperature for 24 days, covering the surface of the component with sawdust ash and sprinkling water for curing are shown in Fig. 4(d).

2.3 Failure modes

As it shown in Figure5, three major failure modes were discovered during the test. They are: Shear-compression failure, Shear-compression failure, Diagonal tension failure.

2.4 Effect of different parameters on behavior of the structure

Among these parameters investigated during the tests, the test results show that the degree of influence of these parameters from large to small in order is: Shear span-to-effective depth ratio, longitudinal reinforcement ratio, section shape, stirrup reinforcement ratio. The Shear span to effective depth ratio is the most influential parameter which determines the failure modes as well as the shear capacity.

3. Existing theory for shear capacity calculation

Shear transfer mechanism can be attributed to the shear force transmitted by uncracked concrete in compression zone, longitudinal reinforcement dowel force, residual tensile stress of concrete on both sides of diagonal crack, as well as concrete acting as compression strut in arch action, and vertical stirrups. Three existing theories (Plastic theory, Strut and Ties theory, Rankine theory) are the most frequently used theory in prediction during the design.

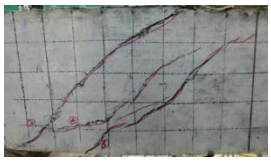

(a) shear-compression failure

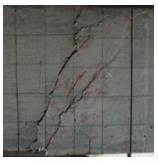

(b) diagonal -compression failure

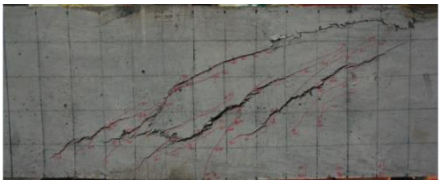

(c) diagonal tension failure

Fig. 5 Major failure modes observed during the tests

Shear transfer mechanism can be attributed to the shear force transmitted by uncracked concrete in compression zone, longitudinal reinforcement dowel force, residual tensile stress of concrete on both sides of diagonal crack, as well as concrete acting as compression strut in arch action, and vertical stirrups. Three existing theories (Plastic theory, Strut and Ties theory, Rankine theory) are the most frequently used theory in prediction during the design.

However, no calculation methods are available in current design codes to calculate the shear capacity of this new type of structures. The experimental tests show that, the failure modes and parameters which influence the shear capacity of high-strength reinforced RPC beams are similar to those of conventional reinforced concrete beams. However, for HSR reinforced RPC concrete, the tensile strength of the concrete and the dosage of the steel fibres both have more significant influence on the shear capacity than normal concrete. Therefore, based on above three existing theories and design codes which have been well applied in reinforced concrete beams, considering the findings from the tests results, the calculation methods for this type of structure are developed.

4. Calculation method based on the plastic theory

The plastic theory method was proposed by Nielson (1984) to analyze the shear behaviour of concrete members. The theory assumes that both reinforcement and concrete are elastic-plastic materials, ignoring the dowel effect of longitudinal reinforcement and compressive stress; for concrete, the yield condition follows the "Mohr-Coulomb" criterion, and ignores the tensile strength of concrete. The plastic theory method considers that when a member starts to fail, it becomes a mobile system consisting of plastic hinges connecting each rigid region. Based on the assumption that the work done by the external force is equal

to the plastic energy consumed inside the member, the plastic work equation is established, and the upper bound solution is obtained.

4.1 Proposed Calculation method

The plastic theory method solves the shear capacity based on material mechanics and provides the upper and lower bound of shear capacity of reinforced concrete beams. Therefore, a new equation is derived based on the plastic theory method and the findings from 23 test results,

According to Lu,1998 and Jiang,1979, as it shown in Figure 6, the yield plane of the beam is composed of two plastic hinges as it shown in dotted line when shear failure occurs. The width of the yield plane is assumed to be 1m. The yielding plane divides the shear and compression zone of members into two parts, I and II, it assumed that no material damage occurs in zone I and II. II slides along the main diagonal crack when the failure occurs.

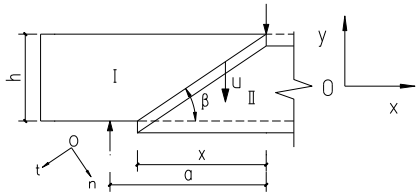

Fig. 6 Failure Mechanism of based on plastic theory

As it shown in Figure 6, the translation at the crack plane can be worked out as (1)

$$\begin{cases} U_x = 0 \\ V_y = u \end{cases} \tag{1}$$

As it shown in Figure 6, for local coordinate n-t, we can get the trains are

$$\begin{cases} \varepsilon_n = U_x sin\beta + V_y cos\beta = ucos\beta \\ \varepsilon_t = 0 \\ \gamma_{nt} = V_y sin\beta + U_x cos\beta = usin\beta \end{cases} \tag{2}$$

So, the principal strain can be determined as follows:

$$\left.\begin{matrix} \varepsilon_1 \\ \varepsilon_2 \end{matrix}\right\} = \frac{\varepsilon_n + \varepsilon_t}{2} \pm \left[(\frac{\varepsilon_n - \varepsilon_t}{2})^2 + (\frac{\gamma_{nt}}{2})^2 \right]^{\frac{1}{2}} = \frac{1}{2} u(\cos\beta \pm 1) \tag{3}$$

When RPC yielding occurs, the yield curve of RPC is located in CD section as shown in Fig. 7. Considering the un-even distribution of compressive stress on plastic hinge line, the effect of steel fibres and the lack of influence of plastic stress-strain relationship on softening effect in failure criterion, the plastic coefficient μ is introduced to obtain the corresponding stress state.

$$\begin{cases} \sigma_1 = (1-\mu) f_t \\ \sigma_2 = -\mu f_c \end{cases} \tag{4}$$

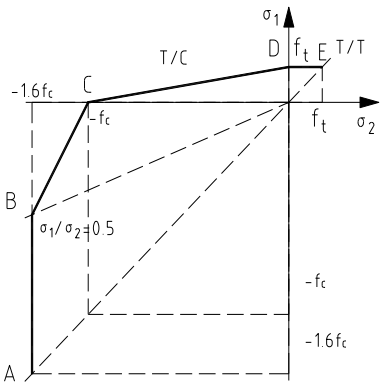

Fig. 7 Constitutive behaviour of RPC concrete

According to energy conservation theorem:

$$W_e = W_c + W_s \tag{5}$$

As

$$W_e = V \cdot V_y = uV \tag{6}$$

And

$$\begin{aligned} W_c &= \int_0^{h\csc\beta} b(\sigma_1\varepsilon_1 + \sigma_2\varepsilon_2)\, dt \\ &= \frac{1}{2}\mu f_c bh \cdot \mu \frac{1-\cos\beta}{\sin\beta} + \frac{1}{2} u f_t bh \cdot (1-\mu) \frac{1+\cos\beta}{\sin\beta} \end{aligned} \tag{7}$$

Also:

$$W_s = u f_{yv} \rho_{sv} bh \cot\beta \tag{8}$$

Substitute (6) ~ (8) into (5) we can obtain:

$$\begin{aligned} V = &\frac{1}{2} f_c bh \cdot \mu \frac{1-\cos\beta}{\sin\beta} + \frac{1}{2} f_t bh \cdot (1-\mu) \frac{1+\cos\beta}{\sin\beta} \\ &+ f_{yv} \rho_{sv} bh \cot\beta \end{aligned} \tag{9}$$

In equation (9), the plastic coefficient μ is deduced from the test results of Cao et al. (2019) to count the plastic effect of RPC and the dowel effect of longitudinal reinforcement. According to the relevant literature Zhao (2005), it can be seen that the plasticity coefficient is influenced primarily by the longitudinal reinforcement ratio and concrete strength f_{cu}, while the shear span ratio has less influence, which can be neglected. Referring to the plasticity coefficient of ordinary concrete beams, the paper deduces the plasticity coefficient of steel fibres reinforced RPC concrete beams using high strength reinforcement, which can consider the influence of steel fibres, such as equation (10):

$$\mu = 1 - 0.009 f_{cu} + 0.155P \tag{10}$$

$$P = 100\rho_s \tag{11}$$

As it is observed from test results of Cao et al (2019), as it shown in the photo of Figure 1 and the failure mechanism diagram shown in Figure 5, the plastic hinge line is more or less connecting the loading point and the support at the final damage state of the test, so it is reasonable to take the

geometrical relation of x≈a, β is shown in equation (12).

$$\arctan(h/a) \le \beta \le \pi/2 \tag{12}$$

According to test result, when β is small, diagonal tensile failure will occur, to get the stationary value of β, it can be worked out as:

$$\frac{dV}{d\beta} = 0 \tag{13}$$

$$\begin{cases} \sin\beta = \dfrac{1}{\sqrt{1+\lambda^2}} \\ \cos\beta = \dfrac{\lambda}{\sqrt{1+\lambda^2}} \end{cases} \tag{14}$$

Where: λ—shear span to depth ration, to simplify we presume $h \approx h_0$, so $\lambda = a/h_0 = a/h$.

Therefore:

$$V = \frac{1}{2} bh_0 \mu f_c (\sqrt{1+\lambda^2} - \lambda) + \frac{1}{2} bh_0 (1-\mu) f_t (\sqrt{1+\lambda^2} + \lambda) + f_{yv} \rho_{sv} \lambda bh_0 \tag{15}$$

The test results show that the shear capacity of T-shaped beams is 15.9%~27% higher than that of rectangular beams. The influence coefficient of flange in reference Cao et al. (2019) is also introduced here. Therefore, the recommended equation for calculating shear capacity based on plastic theory (16) is obtained by introducing the flange influence coefficient α_1

$$V = \frac{1}{2} bh_0 \mu f_c (\sqrt{1+\lambda^2} - \lambda) + \frac{1}{2} bh_0 (1-\mu) f_t (\sqrt{1+\lambda^2} + \lambda) + f_{yv} \rho_{sv} \lambda bh_0 \tag{16}$$

Where: α_1—is 1 for rectangular shape section, is 1.1 for T shape section

4.2 Validation

In order to verify the accuracy of equation (16), the theoretical calculation is validated against the test result of Cao (2019). The validation results are show in Table 6.

The influence of shear span ratio, stirrup ratio, section shape and plastic coefficient is taken into account in the proposed equation (16) based on plastic theory. It can be seen from Table 6 that, the result is in good agreement with experimental results: the mean value of the ratio of experimental values to theoretical values is 1.10, with standard deviation is 0.186 and the coefficient of variation is 16.8%.

5. Calculation method based on Strut and Tie method (STM)

The strut-and-tie Model (STM)model was proposed by Ritter (1899) and improved by Morsch (1909). The model simplifies reinforced concrete beams into articulated truss systems by assuming that the upper chord represents concrete in the compression zone, the lower chord represents longitudinal steel bars under tension and the compressive concrete and stirrups in the cracked reinforced concrete work as the diagonal bars. Vecchio and Collins (1996) discovered the softening phenomenon of concrete struts in the 1980s and proposed the softening constitutive relationship of concrete. In the 1990s, Hsu TTC et al. (1997) proposed corner softening STM model and fixed angle softening model. In the softening model, the equilibrium equation, compatibility condition and the constitutive relation of concrete considering the softening effect are introduced, and the dowel effect are neglected. The softening truss model can reflect the load-bearing condition of members during loading process and obtain accurate shear capacity.

In this section, the method to calculate the shear capacity of this type of new structure based on STM will be presented. This method also considers the failure mechanism of RPC and HSR and the contribution of each component based on the findings for the test results.

5.1 Proposed Calculation method

In order to simplify the calculation, below assumptions are made:

(1) The tensile strength of RPC, dowel effect of longitudinal reinforcement and aggregate interlocking effect between cracks are neglected.

(2) The softening phenomenon of RPC under compression is considered in the model. When the stress of the compressive strut reaches the softening compressive strength, it is considered as component failure.

(3) RPC compression zone is considered as the compression strut, whose stress and strain satisfy Mohr stress circle and Mohr strain circle respectively.

5.1.1 Failure mechanism of RPC

Tests results (Cao et al.2019) show that RPC has softening phenomenon: RPC in shear span is in two-way stress state, and its compressive strength decreases with the increase of tensile strain. The higher the strength of RPC is, the more significant the softening effect is. Therefore, the softening coefficient is introduced in the calculation, as shown in Fig. 8.

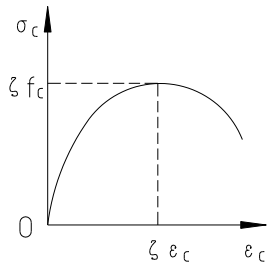

Fig. 8 Strain stress relationship of RPC concrete

Table 6. Validation

	λ	ρ_s/%	ρ_{sv}/%	ρ_{sh}/%	ρ_f/%	Shape of the section	θ_{sv}/°	V_{exp}	V_{cal}	V_{exp}/V_{cal}	Failure pattern
LL1	2.25	6.58	0	0	2	R	—	356.25	387.25	0.92	Shear-compression
LL2	2.25	6.58	0.17	0	2	R	90°	419.25	380.04	1.10	Shear-compression
LL3	2.25	6.58	0.25	0	2	R	90°	430.85	403.86	1.07	Shear-compression
LL4	2.25	6.58	0.58	0	2	R	90°	426.25	502.09	0.85	Flexural failure
LP1	2.25	4.48	0	0	2	R	—	300.5	212.42	1.41	Shear-compression
LP2	2.25	8.18	0	0	2	R	—	425	373.07	1.14	Shear-compression
LH1	1.5	6.58	0	0	2	R	—	656	470.02	1.40	Diagonal compression
LH2	3	6.58	0	0	2	R	—	335	251.92	1.33	Shear-compression
LZ1	1	8.18	0	0	2	R	—	1292	820.90	1.57	Diagonal tension
LZ2	2.25	8.18	0	0	2	R	—	451	391.87	1.15	Shear-compression
LZ3	3.5	8.18	0	0	2	R	—	302	299.66	1.01	Shear-compression
LZ4	1.5	8.18	0.25	0	2	R	90°	681.2	653.15	1.04	Flexural shear failure
LZ5	2.25	8.18	0.25	0	2	R	90°	502.8	500.22	1.01	Shear-compression
LZ6	3	8.18	0.25	0	2	R	90°	409.2	427.80	0.96	Shear-compression
LC1	2.25	8.18	0.50	0	2	R	90°	529.2	580.85	0.91	Flexural shear failure
LC2	3	8.18	0.13	0	2	R	90°	354.6	375.15	0.95	Shear-compression
LC3	3	8.18	0.38	0	2	R	90°	421.7	481.77	0.88	Shear-compression
LY1	3.5	8.18	0	0	2	T	—	384.4	351.10	1.09	Shear-compression
LY2	2.25	8.18	0	0	2	T	—	545.4	459.14	1.19	Shear-compression
LY3	2.25	8.18	0.25	0	2	T	90°	559.8	546.76	1.02	Shear-compression
LT1	1.5	6.58	0.25	0	2	R	90°	585	600.41	0.97	Shear-compression
LT2	1.5	9.87	0.25	0	2	R	90°	774	576.44	1.34	Failure pattern
LT3	2.25	9.87	0.25	0	2	R	90°	523	448.58	1.17	Diagonal compression
Mean										1.10	
standard deviation										0.186	
coefficient of variation										16.8%	

Note : λ is the shear span to depth ratio，ρ_s is the longitudinal rebar ratio，ρ_{sv} is the ratio of the stirrup，ρ_{sh} is the ratio of the web reinforcement, ρ_f is the dosage of steel fibres，θ_{sv} is the angle of the stirrup, R represent rectangular shape, T represents the T shape beam, V_{exp} is test shear capacity，V_{cal} shear capacity from the proposed equation.

So,

$$f_{max} = \zeta \cdot f_c \tag{17}$$

As described in the failure mechanism of the STM, when any location of tie, strut and joint are damaged, the structure fails. When the RPC of the diagonal strut reaches the compressive strength after considering softening effect, the structure reaches the ultimate capacity. The shear capacity of the RPC concrete consists of the shear resistance of RPC, the shear resistance of the steel fibres between the cracks and the shear resistance of the stirrup, as it is shown as follows:

$$V = V_c + V_f + V_s \tag{18}$$

Based on the strain softening of concrete proposed by Vecchio and Collins (1981), the softening coefficient of RPC material is introduced

$$\begin{cases} \sigma_c = \zeta f_c \left[2(\frac{\varepsilon_c}{\zeta\varepsilon_0}) - (\frac{\varepsilon_c}{\zeta\varepsilon_0})^2 \right] & \varepsilon_c / \zeta\varepsilon_0 \le 1 \\ \sigma_c = \zeta f_c \left[1 - (\frac{\varepsilon_c / \zeta\varepsilon_0 - 1}{2/\zeta - 1})^2 \right] & \varepsilon_c / \zeta\varepsilon_0 > 1 \end{cases} \tag{19}$$

according to literature Vecchio and Collins (1981), the softening coefficient can be worked out as

$$\zeta = \frac{1}{0.80 + 0.34\frac{\varepsilon_1}{\varepsilon_0}} \le 1.0 \tag{20}$$

Where,

ε_1 is the principle tensile strain , according to MacGregor (1967), equation 20 can be further transformed into:

$$\zeta = \frac{1}{0.80 + 170\varepsilon_1} \le 0.6 f_c \tag{21}$$

5.1.2 Failure mechanism of High Strength Reinforcement

The bilinear model was used for the high strength reinforcement as it shown in Figure 9, as it is shown from the tests result Cao et al. (2019) that none of the longitudinal bar and stirrup developed into the strain hardening stage.

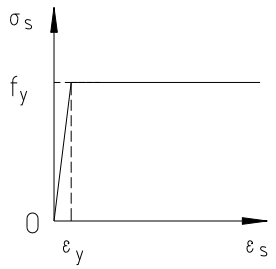

Fig. 9 stain-stress relationship of high strength reinforcement

So, it can be expressed as:

$$\begin{cases} \sigma_y = E_s \varepsilon_s \\ \sigma_y = f_y \end{cases} \tag{22}$$

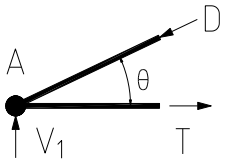

Fig. 10 Equilibrium of the end joints

As shown in Fig. 10, the joint A of the STM model at the support is taken for analysis. In the figure, V1 is the shear force at point A, T is the tensile force of tie, D is the compression force of the strut and the equilibrium equation can be:

$$\begin{cases} V_1 = D\sin\theta \\ T = D\cos\theta \end{cases} \tag{23}$$

$$D = f_{max} bw = \zeta \cdot f_c bw \tag{24}$$

Where：

w—is the height of the strut; *b*—is the width if the strut.

The strain relationship of RPC section after cracking should satisfy the average strain Mohr circle, and the compatibility equation of deformation can be obtained.

$$\begin{cases} \frac{\gamma_{xt}}{2} = (\varepsilon_x - \varepsilon_2) \cdot \cot\theta \\ \frac{\gamma_{xt}}{2} = (\varepsilon_t - \varepsilon_2) \cdot \tan\theta \end{cases} \tag{25}$$

$$\varepsilon_1 + \varepsilon_2 = \varepsilon_x + \varepsilon_t \tag{26}$$

Therefore:

$$\begin{cases} \varepsilon_1 = \varepsilon_x + (\varepsilon_x - \varepsilon_2)\cot^2\theta \\ \varepsilon_2 = \xi \cdot \varepsilon_0 = \frac{0.003}{0.8 + 170\varepsilon_1} \le 0.003 \end{cases} \tag{27}$$

Where,

ε_x—the x component of the strain in the compression strut; θ—the angle between the compression strut and the beam axis.

According to Vecchio and Collins (1981), the value of ε_x is taken as:

at loading position ε_x=0

at support position ε_x=0.5ε_s (ε_s is the strain for the tie)

$$\varepsilon_x = \frac{T}{2E_s A_s} \tag{28}$$

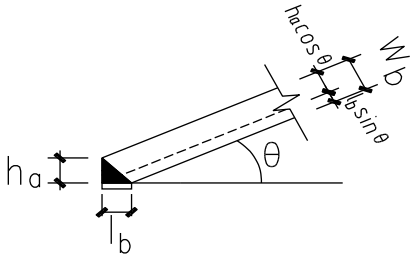

(a)at the support

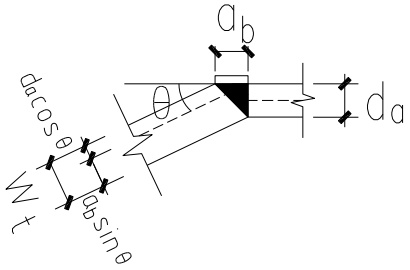

(b)at the loading point

Fig. 11 The angle between the Strut and the beam axis

As it shown in Figure 11 where θ is the angle between the struct and the beam axis.

(1) When no web reinforcement is used, θ is:

$$\tan\theta = (h_0 - 0.5d_a)/a \tag{29a}$$

(2) When web reinforcement is used, θ will not be a fixed value, however, the tests results show that 38°<θ<45°, below empirical equation can be used:

$$\tan\theta = \frac{0.51}{\lambda}\cdot\frac{h}{h_0} \tag{29b}$$

And

$$d_a = 0.45kh_0 \tag{30}$$

$$k = \sqrt{(n\rho_s)^2 + 2n\rho_s} - n\rho_s \tag{31}$$

Where,

n—is the ratio of the Young's module between the reinforcement and RPC concrete Es/Ec;

ρ_s—is the ratio of the longitudinal reinforcement

In addition:

$$w_t = a_b\sin\theta + d_a\cos\theta \tag{32a}$$

$$w_b = l_b\sin\theta + h_a\cos\theta \tag{32b}$$

Where,

a_b—take as 130mm;

l_b—take as 150mm;

h_a—take as h_a=2(h-h_0) ;

h—the depth of the beam ;

h_0—the effective depth of the beam

5.1.3 Shear capacity of RPC beam without web reinforcement

(1) The shear resistance of the upper end of the strut V_t

Solving (20)、(23)、(24)、(29)~(32a), we can get:

$$D_t = \zeta\cdot f_c b w_t = 0.6\cdot f_c b w_t \tag{33}$$

$$V_t = D\cdot\sin\theta = 0.6 f_c b w_t \sin\theta \tag{34}$$

(2) The shear resistance of the upper end of the strut V_b

Solving (21),(23),(24),(27)~(31)、(32b),we can get:

$$V_b = \frac{f_c b w_b}{0.8 + 170\varepsilon_1}\sin\theta \tag{35}$$

$$\varepsilon_1 = \frac{V_b\cot\theta}{2A_sE_s} + \left(\frac{V_b\cot\theta}{2A_sE_s} + \frac{0.003}{0.8+170\varepsilon_1}\right)\cot^2\theta \tag{36}$$

From (35) and (36), we can get:

$$V_b = \frac{2 f_c b w\sin\theta}{0.8 + [0.64 + 680(\frac{f_c b w\cos\theta}{2A_sE_s\sin^2\theta} + 0.003\cot^2\theta)]^{0.5}} \tag{37}$$

So the shear capacity for RPC beam with no web reinforcement are:

$$V_c = \min\{V_t, V_b\} \tag{38}$$

Therefore:

$$\begin{cases} V_t = 0.6 f_c b w_t\sin\theta \\ V_b = \dfrac{2 f_c b w_b\sin\theta}{0.8 + [0.64 + 680\cdot(\frac{f_c b w\cos\theta}{2A_sE_s\sin^2\theta} + 0.003\cot^2\theta)]^{0.5}} \end{cases} \tag{39}$$

5.1.4 Shear resistance of the steel fiber

The steel fibres will enhance the shear resistance, according to Chinese code JGT472-2015, so if the steel fibres is used in the RPC concrete, the resistance of the steel fibres can be worked out as:

$$V_f = \beta_v\lambda_f V_c \tag{40a}$$

$$\lambda_f = \frac{l_f}{d_f}v_f \tag{40b}$$

Where,

β_v—is taken as 0.5 in accordance to Zhao et al. (1992)

λ_f—Characteristic value of steel fiber content
l_f—length of the fibres taken as 13mm;
d_f—diameter of the fibres taken as 0.22mm;
v_f—Volume ratio

5.1.5 Shear resistance of stirrup

The shear resistance of the stirrup is

$$V_s = \sigma_{sv} A_{sv} \frac{a}{s} \tag{41}$$

Considering the uneven for the tensile stress in the stirrup, so taken an extra factor k(λ) (Xu ,2015), k(λ)can be worked through the linear regression of the test result:

$$k(\lambda) = -2.57\lambda^2 + 14.38\lambda - 18.92 \tag{42}$$

Therefore, V_s

$$V_s = k(\lambda) f_{yv} A_{sv} \frac{a}{s} \tag{43}$$

Similar to section 2, to consider the contribution of the flange, for T shape section, the flange factor α_1, is introduced, so

$$V = \alpha_1(1+\beta_v\lambda_f)\cdot\min\{V_t, V_b\} + \alpha_1 k(\lambda) f_{yv} \frac{A_{sv}}{s} a \tag{44}$$

5.2 Validation

The proposed equation (44) based on the STM model takes into account the effects of shear span ratio, longitudinal reinforcement ratio, stirrup ratio, section shape and softening coefficient. From the validation results of Table 7, it can be seen that good agreement is achieved. The mean value of ratio of experimental values to theoretical values is 1.03 with the standard deviation is 0.123 and the coefficient of variation is 12.0%.

6. Calculation of the shear capacity based on Rankine theory

6.1 Proposed Calculation method

It can be observed from the test results of the companion paper Cao et al. (2019) that the diagonal cracks formed in the compression zone of the test beams, and they increase with the increase of load. When the concrete is damaged, shear-compression failure occurs in the compression zone, steel fibress are pulled out in large quantities at the main diagonal cracks, and members are divided into two parts. The internal force diagram is shown in Fig. 12. Its components are: compressive stress σ_c in shear-compression zone, shear stress τ_c in shear-compression zone, aggregate interlocking and friction force

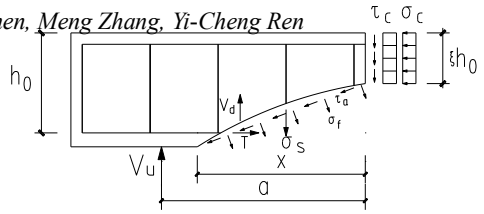

Fig. 12 the internal fore at the crack

τ_a, tensile stress σ_f in steel fibress, stress σ_s in vertical stirrups, dowel force V_d in longitudinal reinforcement and tensile force T in longitudinal reinforcement. Among them, x is the horizontal projection length of the crack, a is the length of the shear span, h0 is the effective height of the section, and ξ is the height coefficient. Therefore, the equilibrium equation can be worked out as:

$$T = \sigma_c b \xi h_0 + \sigma_{fx} + \tau_{ax} \tag{45}$$

$$V = \tau_c b \xi h_0 + V_d + \sigma_{sv} + \sigma_{fy} + \tau_{ay} \tag{46}$$

6.1.1 Basic Assumption

In order to simplify the calculation, the basic assumptions for shear analysis of RPC beams with high strength reinforcement are:

(1) The shear stress and normal stress of concrete in compression zone are uniformly distributed.

(2) The internal force of the beam satisfies the equilibrium theory in inclined plane.

(3) According to the relevant literature Bazant Z P. (1997) and Choi et al. (2007), shear force is mainly provided by the concrete in the shear-compression zone. Because the reactive powder concrete beam does not use coarse aggregate, its aggregate interlocking effect is obviously reduced, so the aggregate interlocking force, friction force and longitudinal bar dowel force of inclined crack surface are neglected.

(4) The stress of steel fiber is neglected. The effect of steel fiber on the coefficient of steel fiber reinforced concrete is considered.

6.2 Rankine theory of failure

Rankine failure criterion is used in this paper. As introduced by Chen (1982), the failure criterion is governed by the maximum principal tensile stress. The stress state of RPC in the shear-compression zone is shown in Figure 13. RPC in the compression zone is affected by shear stress and normal stress. In order to determine the shear resistance, it is necessary to discuss the relationship between the two stresses. Assuming the limit state, the RPC stress satisfies the Mohr circle, as shown in Fig. 14. According to Rankine criterion, the relationship between normal stress and shear stress can be obtained (47).

$$\sigma_1 = \frac{\sigma_u}{2} + \sqrt{(\frac{\sigma_u}{2})^2 + \tau_u^2} \le f_t' \tag{47a}$$

$$\sigma_1 = \frac{\sigma_u}{2} - \sqrt{(\frac{\sigma_u}{2})^2 + \tau_u^2} \le -f_c' \tag{47b}$$

Table 7 validation

	λ	ρ_s/%	ρ_{sv}/%	ρ_{sh}/%	ρ_f/%	Section shape	θ_{sv}/°	V_{exp}	V_{cal}	V_{exp}/V_{cal}	Failure pattern
LL1	2.25	6.58	0	0	2	R	—	356.25	393.12	0.91	Shear-compression
LL2	2.25	6.58	0.17	0	2	R	90°	419.25	414.31	1.01	Shear-compression
LL3	2.25	6.58	0.25	0	2	R	90°	430.85	424.91	1.01	Shear-compression
LL4	2.25	6.58	0.58	0	2	R	90°	426.25	466.47	0.91	Flexural failure
LP1	2.25	4.48	0	0	2	R	—	300.5	382.28	0.79	Shear-compression
LP2	2.25	8.18	0	0	2	R	—	425	402.82	1.06	Shear-compression
LH1	1.5	6.58	0	0	2	R	—	656	719.08	0.91	Diagonal compression
LH2	3	6.58	0	0	2	R	—	335	243.32	1.38	Shear-compression
LZ1	1	8.18	0	0	2	R	—	1292	1341.8	0.96	Diagonal tension
LZ2	2.25	8.18	0	0	2	R	—	451	436.79	1.03	Shear-compression
LZ3	3.5	8.18	0	0	2	R	—	302	289.98	1.04	Shear-compression
LZ4	1.5	8.18	0.25	0	2	R	90°	681.2	734.37	0.93	Flexural shear failure
LZ5	2.25	8.18	0.25	0	2	R	90°	502.8	490.21	1.03	Shear-compression
LZ6	3	8.18	0.25	0	2	R	90°	418.3	382.49	1.09	Shear-compression
LC1	2.25	8.18	0.50	0	2	R	90°	529.2	524.23	1.01	Flexural shear failure
LC2	3	8.18	0.13	0	2	R	90°	354.6	323.83	1.10	Shear-compression
LC3	3	8.18	0.38	0	2	R	90°	421.7	441.15	0.96	Shear-compression
LY1	3.5	8.18	0	0	2	T	—	384.4	318.98	1.21	Shear-compression
LY2	2.25	8.18	0	0	2	T	—	545.4	510.18	1.07	Shear-compression
LY3	2.25	8.18	0.25	0	2	T	90°	559.8	547.60	1.02	Shear-compression
LT1	1.5	6.58	0.25	0	2	R	90°	585	659.17	0.89	Shear-compression
LT2	1.5	9.87	0.25	0	2	R	90°	774	657.74	1.18	Failure pattern
LT3	2.25	9.87	0.25	0	2	R	90°	523	447.58	1.17	Diagonal compression
Mean										1.03	
standard deviation										0.123	
coefficient of variation										12.0%	

Note : λ is the shear span to depth ratio，ρ_s is the longitudinal rebar ratio，ρ_{sv} is the ratio of the stirrup，ρ_{sh} is the ratio of the web reinforcement, $\rho_f$is the dosage of steel fibres，θ_{sv} is the angle of the stirrup, R represent rectangular shape, T represents the T shape beam. V_{exp} is test shear capacity，V_{cal} shear capacity from the proposed equation.

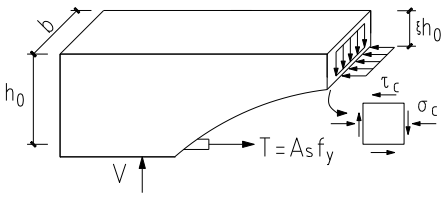

Fig. 13 stress state of the free body

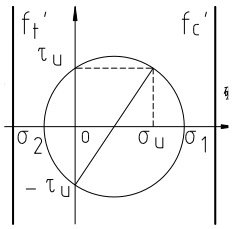

Fig. 14 Rankine failure criteria

Because of the existence of compressive stress, the tensile strength of RPC composite stress state is lower than that of uniaxial tensile strength f_t, and the compressive strength of RPC is the same. In addition, for the beam with shear failure, the value of principal compressive stress is smaller. For simplified calculation, $f_t'=f_t$, $f_c'=0.85f_c$ can be taken. Assuming that the shear bearing capacity is controlled by principal tensile stress, the shear stress and compressive response in shear-compression zone can be obtained by transforming equation (47a). So, the ultimate shear stress:

$$\tau_u(x)=\sqrt{f_t\left[f_t-\sigma_u(x)\right]} \tag{48}$$

Where, x is the distance of the central axis.

$$V=b\int\tau_u(x)dx \tag{49}$$

Considering the average value of the shear stress across the section, so:

$$\overline{\tau_u}=\left[f_t\left(f_t-\overline{\sigma_u}\right)\right]^{\frac{1}{2}} \tag{50}$$

Therefore,

$$V_u=b\int\tau_u(x)dx=b\overline{\tau_u}\xi h_0 \tag{50}$$

After introducing fc′ of RPC, we can get

$$\tau_u/f_c'=\sqrt{(f_t'/f_c')(f_t'/f_c'-\sigma_u/f_c')} \tag{51}$$

In the equation, τ_u and σ_u are shear stress and normal stress of concrete in limit state, respectively. Due to the influence of compressive stress, the tensile strength f_t' under compound stress state is lower than the uniaxial tensile strength f_t; In the same way, due to the influence of tensile

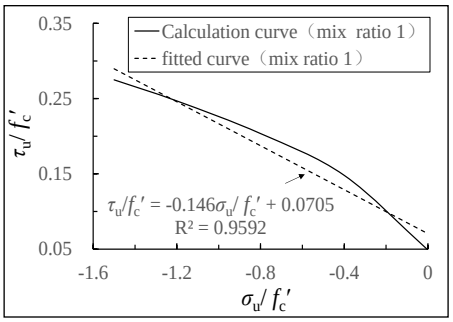

(a) mix ratio 1

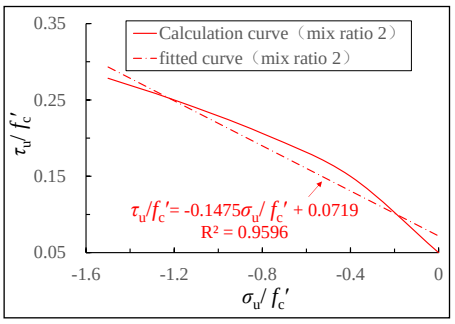

(b) mix ratio 2

Fig. 15 τ_u/f_c' and σ_u/f_c' relation curve

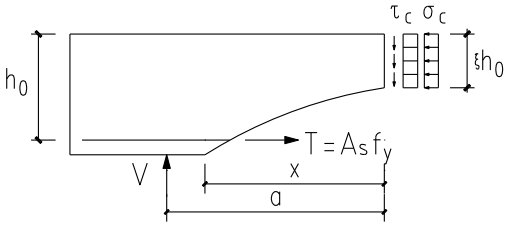

Fig. 16 Free body diagram of RPC beam without web reinforcement

stress, the compressive strength f_c' under the combined stress state is lower than the uniaxial compressive strength f_c. For beams with shear failure, the principal compressive stress is not a large value, so $f_t'=f_t$ and $f_c'=0.85\,f_c$ can be simply taken. According to the basic mechanical properties test of UHPC, f_t and f_c are approximately linear, and $f_t=0.05f_c$(mix ratio 1),$f_t=0.0488f_c$(mix ratio 2)can be taken for simple calculation. According to equation (51), τ_u/f_c' and σ_u/f_c' relationship curve can be drawn, as shown in Fig. 15.

It can be seen from Fig. 15 that there is an approximate linear relationship between them. in order to simplify the calculation, the simplified failure criterion of UHPC in shear-compression zone can be obtained by linearizing equation (49). It can be get:

$$\frac{\tau_u}{f_c'}=A\frac{\sigma_u}{f_c'}+B \tag{52}$$

As can be seen from Fig. 15: Coefficient A and B of mixture ratio 1 are taken as -0.146 and 0.0705 respectively;

Coefficient A and B of mixture ratio 2 are taken as -0.1475 and 0.0719 respectively.

6.2.1 Shear capacity of RPC beam without web reinforcement

For the equilibrium of the free body shown in Fig. 16

$$\Sigma X=0 \qquad \rho_s b h_0 f_y = \sigma_c b \xi h_0 \tag{53}$$

$$\Sigma Y=0 \qquad V = \tau_c b \xi h_0 \tag{54}$$

$$\Sigma M=0 \qquad V \cdot a = \sigma_c b \xi h_0 (h_0 - \xi h_0 / 2) \tag{55}$$

$$\text{And} \qquad \tau_c = A\sigma_c + Bf_c \tag{56}$$

We can get:

$$V = \frac{\rho_s f_y b h_0^{\,2} + A\rho_s^{\,2} f_y^{\,2} b h_0^{\,2} / 2Bf_c}{a + \rho_s f_y h_0 / 2Bf_c} \tag{57}$$

Introducing the shear span ratio λ=a/h0，we can get:

$$V_c = \frac{2B + A\rho_s f_y / f_c}{1 + \dfrac{2Bf_c}{\rho_s f_y} \cdot \lambda} \cdot f_c b h_0 \tag{58}$$

6.2.2 Shear capacity of RPC beam with web reinforcement

Similar to previous section, as it shown in Fig. 17：

$$\Sigma X=0 \qquad \rho_s b h_0 f_y = \sigma_c b \xi h_0 \tag{59}$$

$$\Sigma Y=0 \qquad V = \tau_c b \xi h_0 + \rho_{sv} f_{yv} b x \tag{60}$$

$$\Sigma M=0 \qquad \begin{aligned} V \cdot a &= \sigma b \xi h_0 (h_0 - \xi h_0 / 2) \\ &+ \rho_{sv} f_{yv} b x \cdot x / 2 \end{aligned} \tag{61}$$

$$\tau_c = A\sigma_c + Bf_c \tag{62}$$

Where ：

ρ_{sv}—shear reinforcement ratio；

f_{yv}—yield stress for shear reinforcement ；

x—projection of the crack in x direction, taking as x=0.6λh0；

so

$$V = \frac{2B + A\rho_s f_y / f_c}{1 + 2B\lambda f_c / \rho_s f_y} \cdot f_c b h_0 + \frac{0.6 + 0.36Bf_c}{1 + 2B\lambda f_c / \rho_s f_y} \cdot \frac{f_{yv} A_s}{s} h_0 \tag{63}$$

$$\text{Let} \quad \Psi = \frac{2B + A\rho_s f_y / f_c}{1 + 2B\lambda f_c / \rho_s f_y}, \ \Phi = \frac{0.6 + 0.36Bf_c}{1 + 2B\lambda f_c / \rho_s f_y} \tag{64}$$

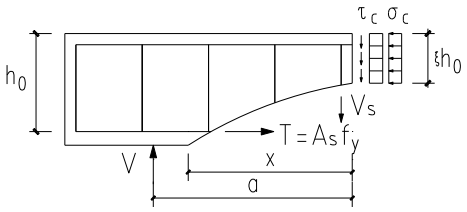

Fig. 17 Free body diagram of RPC beam without web reinforcement

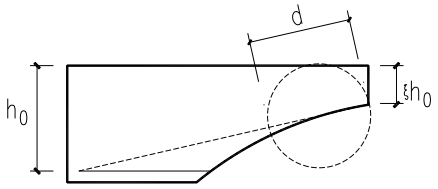

Fig. 18 Principle diagonal cracks at the ultimate state

$$\text{So} \quad V = \Psi f_c b h_0 + \Phi \frac{f_{yv} A_s}{s} h_0 \tag{65}$$

6.2.3 Considering the effect of the flange

As it has been discussed, to consider the contribution of the flange, we can use the flange coefficient α_1，so

$$V = \alpha_1 \Delta f_c b h_0 \tag{66}$$

Where ：

$$\Delta = \frac{2B + A\rho_s f_y / f_c + 0.6\rho_{sv} f_{yv} / f_c + 0.36B\rho_{sv} f_{yv}}{1 + 2B\lambda f_c / \rho_s f_y}$$

α_1—is 1 for rectangular shape section or is 1.1 for T shape section.

6.2.4 Size effect

The shear resistance of the concrete beam will reduce when the size of the beam increase (Cevik et al.,2009, Gulsan et al.,2018) flowing the research of Hasegawa et al (1985)

$$\sigma_n = (1.2 - 1.3d) f_t \tag{67}$$

As it shown in Fig. 18, we take d=0.16a (a is the shear span length), so we can get

$$\sigma_n = (1.2 - 0.2a) f_t \tag{68}$$

So it can be further developed as :

$$V = \alpha_1 (1.2 - 0.2a) \Delta f_c b h_0 \tag{69}$$

Table 8 Validation

	λ	ρ_s/%	ρ_{sv}/%	ρ_{sh}/%	ρ_f/%	Section shape	V_{exp}	V_{cal}	V_{cal}/V_{exp}	Failure pattern
LL1	2.25	6.58	0	0	2	R	356.25	383.36	0.93	Shear-compression
LL2	2.25	6.58	0.17	0	2	R	419.25	430.97	0.97	Shear-compression
LL3	2.25	6.58	0.25	0	2	R	430.85	450.13	0.96	Shear-compression
LL4	2.25	6.58	0.58	0	2	R	426.25	438.82	0.97	Flexural failure
LP1	2.25	4.48	0	0	2	R	300.50	310.42	0.97	Shear-compression
LP2	2.25	8.18	0	0	2	R	425.00	415.17	1.02	Shear-compression
LH1	1.5	6.58	0	0	2	R	656.00	648.09	1.01	Diagonal compression
LH2	3	6.58	0	0	2	R	335.00	321.62	1.04	Shear-compression
LZ1	1	8.18	0	0	2	R	648.00	600.6	1.08	Diagonal tension
LZ2	2.25	8.18	0	0	2	R	451.00	426.64	1.06	Shear-compression
LZ3	3.5	8.18	0	0	2	R	302.00	339.44	0.89	Shear-compression
LZ4	1.5	8.18	0.25	0	2	R	681.00	677.94	1.00	Flexural shear failure
LZ5	2.25	8.18	0.25	0	2	R	502.80	486.39	1.03	Shear-compression
LZ6	3	8.18	0.25	0	2	R	418.30	471.2	0.89	Shear-compression
LC1	2.25	8.18	0.50	0	2	R	529.20	559.32	0.95	Flexural shear failure
LC2	3	8.18	0.13	0	2	R	354.60	415.14	0.85	Shear-compression
LC3	3	8.18	0.38	0	2	R	421.70	462.38	0.91	Shear-compression
LY1	3.5	8.18	0	0	2	T	384.40	414.36	0.93	Shear-compression
LY2	2.25	8.18	0	0	2	T	545.40	526.14	1.04	Shear-compression
LY3	2.25	8.18	0.25	0	2	T	559.80	545.31	1.03	Shear-compression
LT1	1.5	6.58	0.25	0	2	R	585.00	630.81	0.93	Shear-compression
LT2	1.5	9.87	0.25	0	2	R	774.00	808.4	0.96	Failure pattern
LT3	2.25	9.87	0.25	0	2	R	523	537.55	0.97	Diagonal compression
Mean									0.97	
standard deviation									0.061	
coefficient of variation									6.12%	

Note： λ is the shear span to depth ratio，ρ_s is the longitudinal rebar ratio，ρ_{sv} is the ratio of the stirrup，ρ_{sh} is the ratio of the web reinforcement, ρ_f is the dosage of steel fibres，θ_{sv} is the angle of the stirrup, R represent rectangular shape, T represents the T shape beam. V_{exp} is test shear capacity，V_{cal} shear capacity from the proposed equation

6.3 Validation

Equation (69) is based on the ultimate equilibrium theory of inclined plane. The effects of shear span ratio, stirrup ratio, longitudinal reinforcement ratio and cross-section shape are comprehensively considered. From Table 8, it can be seen that good agreement is achieved. The mean value of ratio of experimental values to theoretical values is 0.97 with the standard deviation is 0.061 and the coefficient

of variation is 6.12%.

7. Parameter affecting the accuracy of the prediction

7.1 Shear span ratio

The influence of shear span ratio is directly taken into account in all the three equations, and the calculated results of shear capacity decrease with the increase of shear span ratio, which is consistent with the experimental results. The predicted results of the plastic theory are too conservative for the beams without web reinforcement with small shear span ratio; The proposed model using Strut and Tie and Rankine Theory can accurately predict the beams without web reinforcement. But the predicted results of Strut and Tie of beam shear span ratio change are better than the other two theoretical proposals. The three theories can predict the whole test beam with web reinforcement better. The comparison results are shown in Fig. 19 and 20.

7.2 Ratio of longitudinal reinforcement

Fig. 21 and 22 are curves of shear capacity vs longitudinal reinforcement ratio of beams without and with web reinforcement, respectively. The prediction of Rankine theory is the best in the three theories. The influence of various longitudinal reinforcement ratio is directly taken into account in Rankine theory. However, plastic theory indirectly reflects the influence of longitudinal reinforcement ratio through plastic coefficient μ, while the softening Strut and Tie model reflects the effect of longitudinal reinforcement in section height w. When P=4.48% The predicted results of the plastic theory for beams without web reinforcement are conservative. The Strut and Tie model is also worse for the prediction of beams without web reinforcement. In addition, for LT3 with higher longitudinal reinforcement ratio (ρ=9.87%, ρ_{sv}=0.25%), plastic theory and Strut and Tie are conservative in prediction. The comparison results are shown in Fig. 21 and 22.

7.3 Stirrup ratio

All the three theories can directly reflect the role of stirrup ratio, and the calculated shear capacity increases with the increase of stirrup ratio, which is in good agreement with the experimental law. Therefore, the three theoretical equations can well predict the shear capacity when the stirrup ratio changes. When the stirrup ratio is increased to 0.50%, the member will be transformed into bending-shear failure; when the stirrup ratio is 0.58%, the member will be transformed into bending failure. The discrepancy is noticed in predicted results of the proposed plasticity theory under both failure modes. The model of Strut and Tie is the best before bending failure, while the Rankine theory can accurately predict the stirrup ratio when the stirrup ratio is high. The comparison results are shown in Fig. 23.

7.4 Shape of the cross-section

The influence of flange is taken into account in the three equations, and the flange coefficient is used to modify the proposed equations. Plastic theory is less sensitive to the influence of flange, and the addition of flange coefficient cannot improve the prediction, which indicates that the flange influence coefficient needs to be further improved. For the other two theories, the calculation results are close to the test results. Therefore, Flange is an important factor affecting the shear capacity of RPC beams. The comparison results are shown in Fig. 24-27.

7.5 Discussion

Based on the findings from the test result, three theories are used to develop the calculation method to predict the shear capacity of HSR reinforced RPC beams. The proposed three calculation models are validated against test results. The validation results show that all the three theories can accurately predict the shear capacity of HSR reinforced RPC beams. The overall results show that the Rankine theory and the softened Strut and Tie model provides better shear capacity prediction. The plastic theory can predict the shear capacity of beams with web reinforcement better, but it is conservative for beams without web reinforcement.

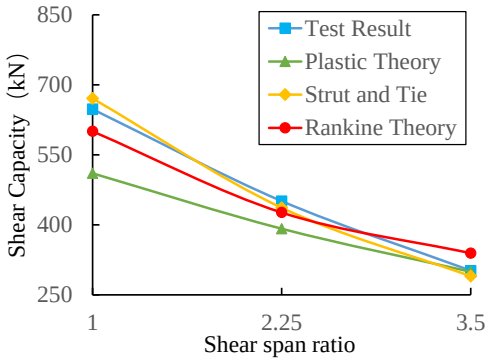

Fig. 19 Shear capacity V.S. Shear span ratio of beam without web reinforcement

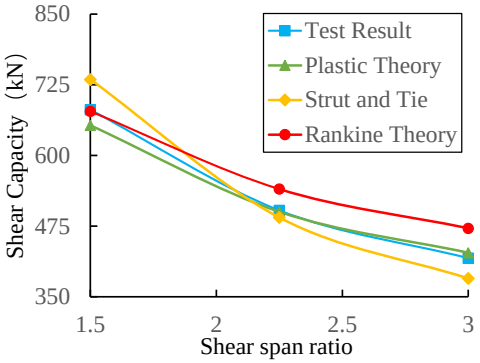

Fig. 20 Shear capacity V.S. Shear span ratio of beam with web reinforcement

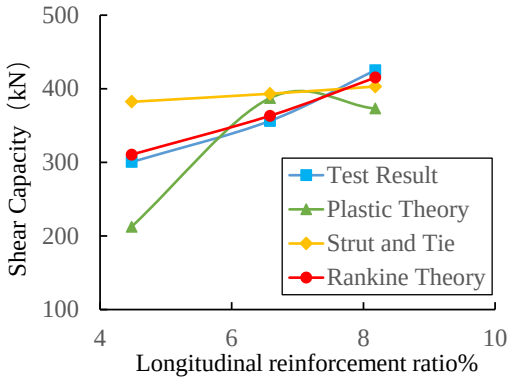

Fig. 21 Shear capacity V.S. Longitudinal reinforcement ratio of beam without web reinforcement

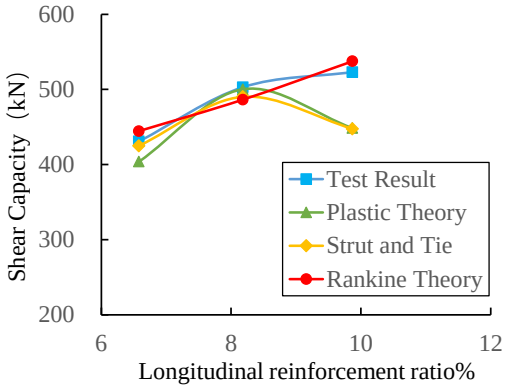

Fig. 22 Shear capacity V.S. Longitudinal reinforcement ratio of beam with web reinforcement

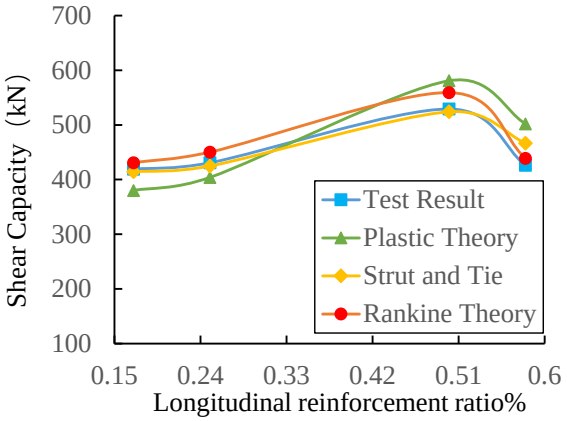

Fig. 23 Shear capacity V.S. Stirrup ratio

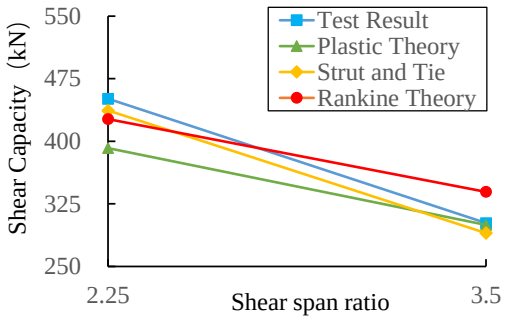

Fig. 24 Shear capacity V.S. Shear span ratio of rectangular shape beam

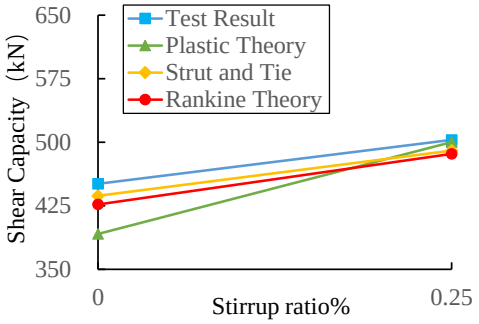

Fig. 25 Shear capacity V.S. Stirrup ratio of rectangular shape beam

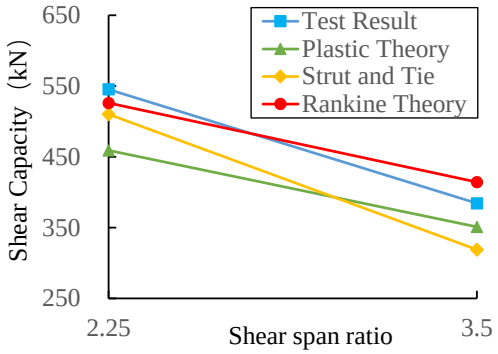

Fig. 26 Shear capacity V.S. Shear span ratio of T shape beam

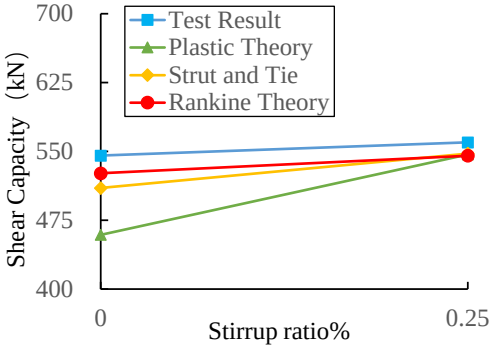

Fig. 27 Shear capacity V.S. Stirrup ratio of T shape beam

All three theories can be used to predict the shear capacity considering the influence of shear span ratio, stirrup ratio and Shape of the cross-section. They are generally good for predicting shear-compression failure, bending-shear failure or diagonal shear failure of beams. For beams with diagonal compression failure, the predictions of three theories are conservative. For beams with flexural failure, the prediction results of the three theories deviate greatly. For the plastic theory, the calculated value first increases and then decreases with the increase of longitudinal reinforcement ratio, which is different from the actual trend. It is only applicable to the test beams with moderate longitudinal reinforcement ratio (ρ_s=6.58%~8.18%). The variation trend of calculated value with stirrup ratio is consistent with the actual situation, but its accuracy is worse than the other two theories. The prediction results of rectangular beams with added flanges are slightly conservative and still within the acceptable range. For strut and Tie model: The prediction results of test beams with and without web reinforcement are generally good. The predicted results are better when shear span ratio, stirrup ratio and cross-section shape change. It is unsafe to predict when the longitudinal reinforcement ratio is small, which is suitable for test beams with longitudinal reinforcement ratio of 6.58%~8.18%. For the Rankine theory, the prediction results of test beams with and without web reinforcement are generally good. The prediction results of shear span ratio, longitudinal reinforcement ratio, stirrup ratio and section shape change are good.

8. Conclusions

In this paper, based on the tests result, calculation methods to predict the shear capacity of this new type of beams were first time developed.

The main findings are as follows:

- Among these parameters investigated during the tests, the test results show that the degree of influence of these parameters from large to small in order is: Shear span-to-effective depth ratio, longitudinal reinforcement ratio, section shape, stirrup reinforcement ratio. The Shear span to effective depth ratio is the most influential parameter which determines the failure modes as well as the shear capacity.
- According to the plastic theory, the equilibrium equation was established based on the principle of virtual work, and the influence of plastic coefficient and section shape was considered. The calculation result is satisfactory but conservative. The suggested equation is applicable to beams with web reinforcement, the influence of shear span ratio and stirrup reinforcement ratio is well predicted, which can be used as for the design of beams with web reinforcement.
- Based on existing strut-and-tie model, considering the softening effect of RPC, the failure criterion for HSR reinforced RPC beams was established. The calculation results are in good agreement with test results. Compared with the other two theories, the softened strut-and-tie model can better predict the influence of shear span ratio on the beam without web reinforcement. In addition, the influence of stirrup reinforcement ratio and section shape change is well predicted, which is suitable for the engineering design.
- The equation derived from Rankine theory is better than the other two theories in predicting the influence of longitudinal reinforcement ratio. The prediction results of the effect of stirrup reinforcement ratio is better, and the influence of shear span ratio and section shape is good. It is suitable for engineering design.

Acknowledgments

This research was financially supported by the National Natural Science Foundation of China (Grant No. 51368013) and Guangxi Key Laboratory of Green Building Materials and Construction Industrialization (No. 19-J-21-6), The authors wish to acknowledge the sponsors. However, any opinions, findings, conclusions and recommendations presented in this paper are those of the authors and do not necessarily reflect the views of the sponsors.

References

Baby F., Marchand P and Atrach M., Toutlemonde F. (2013), "Analysis of flexure-shear behavior of UHPFRC beams based on stress field approach", *Engineering Structures*, Volume **56** 194–206. https://doi.org/10.1016/j.engstruct.2013.04.024.

Baby F., Marchand P. and Toutlemonde F. (2014), "Shear Behavior of Ultrahigh Performance Fiber-Reinforced Concrete Beams. I Experimental Investigation", *Journal of Structural Engineering*, **140**(5). https://doi.org/10.1061/(ASCE)ST.1943-541X.0000907.

Bazant Z P. (1997), "Fracturing truss model: size effect in shear failure of reinforced concrete", *Journal of Engineering Mechanics*, **123**(12):1276-1288. https://doi.org/10.1061/(ASCE)0733-9399(1997)123:12(1276).

Cao, X., Deng, X.-F., Jin, L.-Z., Fu, F. and Qian, K. (2021), "Shear capacity of reactive powder concrete beams using high-strength steel reinforcement. Proceedings of the Institution of Civil Engineers", *Structures and Buildings*, **174**(4), pp. 276–291. https://doi.org/10.1680/jstbu.19.00051.

Chen B. (2007), "Study on Shear Behavior of Prestressed RPC Beams", Master Thesis, Changsha: Hunan University, China.

Choi K, Park H and Wight J K. (2007), "Unified shear strength model for reinforced concrete beams-Part I: Development", *ACI Structural Journal*,**104**:142-152. https://doi.org/10.14359/18526.

Deng Z., Jumbe R.D. and Yuan C. (2014), "Bonding between high strength rebar and Reactive Powder Concrete", *Computers and Concrete*, **13**: 411-421. https://doi.org/10.12989/CAC.2014.13.3.411.

Deng Z.C., Zhou D.Z., Cheng S.K. (2014), "Shear capacity of reinforced RPC beams", *Journal of Harbin University of Engineering*, **12**:1512-1518.

Ghosh P., Konečný P., Lehner P. and Tikalsky P. (2017), "Probabilistic time-dependent sensitivity analysis of HPC bridge deck exposed to chlorides", *Computers and Concrete*, Vol.**19**, Number 3, pages 305-313. http://dx.doi.org/10.12989/cac.2017.19.3.305.

Abdulhaleem K. , Gülşan Eren , Cevik Abdulkadir and Kurtoglu,

Ahmet. (2018), "Size effect on strength of Fiber-Reinforced Self-Compacting Concrete (SCC) after exposure to high temperatures", *Computers and Concrete*. **21**. 681-695. https://doi.org/10.12989/cac.2018.21.6.681.

Hasegawa T, Shioya T, Okada T. (1985), "Size effect on splitting tensile strength of concrete", *Proceedings of the 7th Conference of the Japan Concrete Institute*, Japan, June.

Hoang A.L., and Fehling E. (2017), "Numerical analysis of circular steel tube confined UHPC stub columns", Computers and Concrete, Vol **19**, Number 3, pages 263-273. https://doi.org/10.12989/cac.2017.19.3.000.

Hsu, T.T.C., Zhang and L.X. (1997), "Nonlinear Analysis of Membrane Elements by Fixed Angle Softened-Truss Model", *ACI Structural Journal*, **94**(5):483-492. https://doi.org/10.14359/498.

Jiang D.H. (1979), "Plastic solution of shear strength of reinforced concrete beams" Journal of Tongji University, 1979 (05): 29-43.

Kang P. (2012), "Design and calculation methods of reactive powder concrete members under bending, shearing and compression", Master Thesis, Beijing Jiaotong University, Beijing, China.

Lai J., Sun W., (2010), "Dynamic tensile behaviour of Reactive Powder Concrete by Hopkinson bar experiments and numerical simulation". *Computers and Concrete*, Vol. **7** No. 1. https://doi.org/10.12989/cac.2010.7.1.083.

Marcinczak D., Trapko T and Musiał M. (2019), "Shear strengthening of reinforced concrete beams with PBO-FRCM composites with anchorage", *Composites Part B: Engineering*" Volume **158**, Pages 149-161. https://doi.org/10.1016/j.compositesb.2018.09.061.

Morsch E. (1909), "Concrete Steel Construction (English translation of "Der Eisenbetonbau",1902). McGraw-Hill , New York , 1909.

Nematzadeh M. and Poorhosein R. (2017), "Estimating properties of Reactive Powder Concrete containing hybrid fibers using UPV", *Computers and Concrete*, Vol. **20** No. 4. https://doi.org/10.12989/cac.2017.20.4.491.

Nielsen, M.P.(1984), "Limit Analysis and Concrete Plasticity", New Jersey : Prentice-Hall. Inc. Englewwood Cliffs, New Jersey, USA.

Poorhosein R. and Nematzadeh M. (2018), "Mechanical behavior of hybrid steel-PVA fibers reinforced Reactive Powder Concrete", *Computers and Concrete*, An Int'l Journal Vol. **21** No. 2. https://doi.org/10.12989/cac.2018.21.2.167.

Pourbaba M., Joghataie A., Mirmiran A. (2018), "Shear behavior of ultra-high performance concrete", *Construction and Building Materials*, **183**: 554–564. https://doi.org/10.1016/J.CONBUILDMAT.2018.06.117.

Qi J, Ma Z J, Wang J (2016), "Shear Strength of UHPFRC Beams: Mesoscale Fiber-Matrix Discrete Mode", *Journal of Structural Engineering*, 04016209. https://doi.org/10.1061/(ASCE)ST.1943-541X.0001701.

Ridha M., Al-Shaarbaf I., Sarsam K. (2018), "Experimental study on shear resistance of reactive powder concrete beams without stirrups", *Mechanics of Advanced Materials and Structures*, 1537-6494. https://doi.org/10.1016/j.cscm.2018.03.002.

Ridha, M. M. S., Al-Shaarbaf, I. A. S., & Sarsam, K. F. (2018), "Experimental study on shear resistance of reactive powder concrete beams without stirrups", *Mechanics of Advanced Materials and Structures*, **27**(12), 1006–1018. https://doi.org/10.1080/15376494.2018.1504258.

Ridha, Maha MS, Kaiss F. Sarsam, and Ihsan AS Al-Shaarbaf (2018), "Experimental Study and Shear Strength Prediction for Reactive Powder Concrete Beams", *Case studies in construction materials*, Volume **8**: 434-446. https://doi.org/10.1016/j.cscm.2018.03.002.

Ritter.W., (1899), Die bauweise Hennebique. Schweizeitung, Zurich.

Sifatullah B., Adekunle S.K and Al-Osta M., (2018), "Numerical investigation of the shear behavior of reinforced ultra-high-performance concrete beams", *Structural Concrete*, **19**:305–317. https://doi.org/10.1002/suco.201700062.

Talayeh Noshiravani and Eugen Brühwiler (2014), "Analytical Model for Predicting Response and Flexure-Shear Resistance of Composite Beams Combining Reinforced Ultrahigh Performance Fiber-Reinforced Concrete and Reinforced Concrete", *Journal of Structural Engineering*, **140**(6): 04014012 https://doi.org/10.1061/(ASCE)ST.1943-541X.0000902.

Tamás Mészöly, Norbert Randl (2018), "Shear behavior of fiber-reinforced ultra-high performance concrete beams", *Engineering Structures*, **168**:119–127. https://doi.org/10.1016/j.engstruct.2018.04.075.

Thiemicke J., Fehling E. (2016), "Proposed Model to predict the Shear Bearing Capacity of UHPC-Beams with Combined Reinforcement", *Proc. 4th International Symposium on Ultra-High Performance Concrete and High Performance Construction Materials*, Kassel, Germany, March.

Tung N. D., Tue N. V. (2018), "Shear resistance of steel fiber-reinforced concrete beams without conventional shear reinforcement on the basis of the critical shear band concept", *Engineering Structures*, Volume **168**, Pages 698-707. https://doi.org/10.1016/j.engstruct.2018.05.014.

Vecchio F. J. and Collins M. P. (1996), "Analytical model for shear critical reinforced-concrete members", *Journal of Structural Engineering*, **122**(9):1123-1124. https://doi.org/10.1061/(ASCE)0733-9445(1996)122:12(1459).

Withit Pansuk, Thuc N. Nguyen and Yasushiko Sato. (2017), "Shear capacity of high performance fiber reinforced concrete I-beams", *Construction and Building Materials*, **157**: 182–193. https://doi.org/10.1016/j.conbuildmat.2017.09.057.

Woo-Young Lim, and Sung-Gul Hong. (2016), "Shear Tests for Ultra-High Performance Fiber Reinforced Concrete (UHPFRC) Beams with Shear Reinforcement", *International Journal of Concrete Structures and Materials*, Vol.**10**(2):177–188. https://doi.org/10.1007/s40069-016-0145-8.

Wu X.G., Han S.M. (2009), "First diagonal cracking and ultimate shear of I-shaped reinforced girders of ultra high-performance fiber reinforced concrete without stirrup", *International Journal of Concrete Structures and Materials*, Vol.**3**(1): 47-56. https://doi.org/ 10.4334/IJCSM.2009.3.1.047 .

Xia Z.X. (2007), "Study on inclined plane shear capacity of reactive powder concrete beams", Master Thesis, Beijing Jiaotong University, Beijing, China.

Yan J.P. (2011), "Experimental study on shear strength of reactive powder concrete", Master Thesis, Beijing Jiaotong University, Beijing, China.

Yen Lei Voo, Wai Keat Poon, and Stephen J. (2010), "Foster Shear Strength of Steel Fiber-Reinforced Ultrahigh Performance Concrete Beams without Stirrups", *Journal of Structural Engineering*, **136**(11): 1393-1400. https://doi.org/10.1061/(ASCE)ST.1943-541X.0000234.

Zhao J., Gao D.Y. and Zhu H.T (2005), "Plastic limit analysis of shear capacity of oblique section of steel fiber reinforced concrete beams", *Quarterly Journal of Mechanics*, **2**: 235-240.